JACC: CARDIOVASCULAR IMAGING VOL. 10, NO. 10, 2017

ISSN 1936-878X/$36.00
PUBLISHED BY ELSEVIER
http://dx.doi.org/10.1016/j.jcmg.2016.11.016

Serial Assessment of Tissue Precursors and Progression of Coronary Calcification Analyzed by Fusion of IVUS and OCT

5-Year Follow-Up of Scaffolded and Nonscaffolded Arteries

Yaping Zeng, MD, PhD,[a,b] Hiroki Tateishi, MD, PhD,[a] Rafael Cavalcante, MD, PhD,[a] Erhan Tenekecioglu, MD,[a] Pannipa Suwannasom, MD,[a,c] Yohei Sotomi, MD,[c] Carlos Collet, MD,[c] Shaoping Nie, MD, PhD,[b] Hans Jonker, BSc,[d] Jouke Dijkstra, MD, PhD,[e] Maria D. Radu, MD, PhD,[a,f] Lorenz Räber, MD, PhD,[a,g] Dougal R. McClean, MD,[h] Robert-Jan van Geuns, MD, PhD,[a] Evald H. Christiansen, MD, PhD,[i] Therese Fahrni, RN,[j] Jacques Koolen, MD, PhD,[k] Yoshinobu Onuma, MD, PhD,[a] Nico Bruining, PhD,[a] Patrick W. Serruys, MD, PhD[l]

ABSTRACT

OBJECTIVES The aim of this study was to assess calcium growth with fused grayscale intravascular ultrasound (IVUS), IVUS-virtual histology, and optical coherence tomography (OCT) from baseline to 5-year follow-up in patients treated with bioresorbable vascular scaffolds.

BACKGROUND IVUS and OCT have individual strengths in assessing plaque composition and volume. Fusion of images obtained using these methods could potentially aid in coronary plaque assessment.

METHODS Anatomic landmarks and endoluminal radiopaque markers were used to fuse OCT and IVUS images and match baseline and follow-up.

RESULTS Seventy-two IVUS-virtual histology and OCT paired matched cross-sectional in- and out-scaffold segments were fused at baseline and follow-up. In total, 46 calcified plaques at follow-up were detected using the fusion method (33 in-scaffold, 13 out-scaffold), showing either calcium progression (52.2%) or de novo calcifications (47.8%). On OCT, calcification volume increased from baseline to follow-up by 2.3 ± 2.4 mm^3 ($p = 0.001$). The baseline virtual histologic tissue precursors of dense calcium at follow-up were necrotic core in 73.9% and fibrous or fibrofatty plaque in 10.9%. In 15.2%, calcium was already present at baseline. Precursors on OCT were lipid pool in 71.2%, fibrous plaque in 4.3%, and fibrocalcific plaque in 23.9%.

CONCLUSIONS The use of OCT and IVUS fusion imaging shows similar calcium growth in- and out-scaffold segments. Necrotic core is the most frequent precursor of calcification. The scaffold resorption process creates a tissue layer that re-caps the calcified plaques. (Absorb Clinical Investigation, Cohort B [ABSORB B]; NCT00856856) (J Am Coll Cardiol Img 2017;10:1151–61) © 2017 by the American College of Cardiology Foundation.

From the [a]ThoraxCentre, Erasmus Medical Center, Rotterdam, the Netherlands; [b]The Emergency & Critical Care Center of Beijing Anzhen Hospital, Capital Medical University, Beijing, the People's Republic of China; [c]Academic Medical Center, Amsterdam, the Netherlands; [d]Cardialysis BV, Rotterdam, the Netherlands; [e]Division of Image Processing, Department of Radiology, Leiden University Medical Center, Leiden, the Netherlands; [f]Department of Cardiology, Rigshospitalet, Copenhagen, Denmark; [g]Department of Cardiology, Bern University Hospital, Bern, Switzerland; [h]Department of Cardiology, Christchurch Hospital, Christchurch, New Zealand; [i]Department of Cardiology, Aarhus University Hospital, Skejby Hospital, Aarhus, Denmark; [j]Department of Cardiology, Swiss Cardiovascular Center, University Hospital, Bern, Switzerland; [k]Cardiology, Catharina Ziekenhuis, Eindhoven, the Netherlands; and the [l]International Centre for Circulatory Health, Imperial College, London, United Kingdom. Drs. Räber, Onuma, and Serruys are members of the advisory board of Abbott Vascular. Dr. Zeng was sponsored by Abbott Vascular. All other authors have reported that they have no relationships relevant to the contents of this paper to disclose. Drs. Zeng and Tateishi contributed equally to this work.

Manuscript received August 2, 2016; revised manuscript received October 7, 2016, accepted November 10, 2016.

ABBREVIATIONS AND ACRONYMS

BVS = bioresorbable vascular scaffold

DC = dense calcium

GS = grayscale

IQR = interquartile range

IVUS = intravascular ultrasound

NC = necrotic core

OCT = optical coherence tomography

ROI = region of interest

VH = virtual histology

Coronary atherosclerotic plaque characterization with intravascular imaging is important for assessing atherosclerosis, planning percutaneous coronary interventions, and predicting outcomes (1). Intravascular ultrasound (IVUS) and optical coherence tomography (OCT) are the 2 most widely used intracoronary imaging techniques.

The main advantage of IVUS lies in its deep penetration ability, which offers a cross section of the entire vessel wall and allows the detection of deep calcification. Its main disadvantages are limited resolution and the strong reflection of the ultrasound waves by endoluminal calcium, which creates a shadow behind the calcium that precludes assessment of the extent and depth of calcification (2).

SEE PAGE 1162

IVUS-virtual histology (VH) increases the usefulness of IVUS by characterizing tissue components and allowing better risk stratification (1). However, stent and scaffold struts are incorrectly recognized as dense calcium (DC) surrounded by necrotic core (NC) on VH. Moreover, the VH algorithm also incorrectly inputs fibrofatty signal in the shadow behind DC (3,4).

OCT enables a detailed assessment of near-lumen plaque characteristics because of its high resolution (10 to 20 μm), including features related to plaque vulnerability such as thin fibrous caps. OCT can also assess calcifications more accurately because the light can cross calcified areas without being excessively reflected and without substantial attenuation, allowing visualization of the real extent of calcification plaque along its longitudinal and axial distribution, at least in the relatively superficial layer of the vessel wall (5). However, the high resolution comes at the cost of limited depth of penetration (6). Therefore, OCT is unable to detect deep calcium.

The feasibility and advantages of combining the individual strengths of both technologies in vivo have been described (7). The feasibility of off-line fusion images of coregistered IVUS and OCT has been previously described (8).

The objective of the present study was to comprehensively assess the serial progression of calcification at 5-year follow-up after bioresorbable vascular scaffold (BVS) implantation using matched fusion images from IVUS and OCT. We sought to evaluate calcium progression and describe the baseline tissue precursors of calcification at long-term follow-up.

METHODS

STUDY DESIGN. In Cohorts B1 and B2 from ABSORB (Absorb Clinical Investigation) (n = 101), 28 patients with 29 lesions underwent IVUS and OCT assessment at baseline and 5 years (9) (Online Figure 1). OCT, grayscale (GS)-IVUS, and IVUS-VH images were displayed simultaneously and screened concomitantly frame by frame to match using radiopaque markers and/or anatomic marks at each time point (Online Figure 2). Then the matched cross sections selected were colocalized between 2 time points. Each cross section was subdivided into 4 quadrants, and the presence of each type of atherosclerotic plaque was assessed in each quadrant (7).

GS-IVUS ACQUISITION. Post-implantation and 5-year images were obtained using 20-MHz, phased-array IVUS catheters (Eagle Eye, Volcano, Rancho Cordova, California) using an automated pull-back of 0.5 mm/s. Semiautomatic detection of both lumen and external elastic membrane was performed using QCU-CMS-Research software version 4.69 (Medis Medical Imaging, Leiden, the Netherlands). Calcification on GS-IVUS was defined as bright echoes with acoustic shadowing (2).

IVUS RADIOFREQUENCY ANALYSIS. On IVUS-VH analysis, "pseudo" DC or NC related to the scaffold strut was defined as confluent, uninterrupted white color surrounded by red color, located near the lumen contour. DC located behind the struts and separated from the struts was considered as real DC at baseline (10). The "white color" was then defined as calcification if the confluent white-color area exceeded 0.0625 mm^2 (0.25 × 0.25 mm), considering the resolution of the 20-MHz IVUS catheters used in the study (2). To determine the major baseline tissue precursor of calcifications at 5 years, fusion images weighting VH information in topographically matched calcified areas at follow-up were used. The baseline VH tissue precursor was determined as the major tissue component, if it constituted approximately 50% of the total tissue.

OCT IMAGE ACQUISITION AND ANALYSIS. OCT acquisition was performed using C7/C8 frequency domain systems (Light Lab Imaging, Westford, Massachusetts) (11). The OCT images acquired at baseline and follow-up were analyzed off-line at 100- or 200-μm longitudinal intervals within the region of interest (ROI) using QCU-CMS.

Three tissue components were identified on the basis of consensus of 5 analysts: fibrous, fibrocalcific, and lipid pool (lipid or NC) (11) (Online Appendix). The baseline OCT tissue precursor of calcifications at

FIGURE 1 Matching and Fusion Method in ABSORB Cohort B

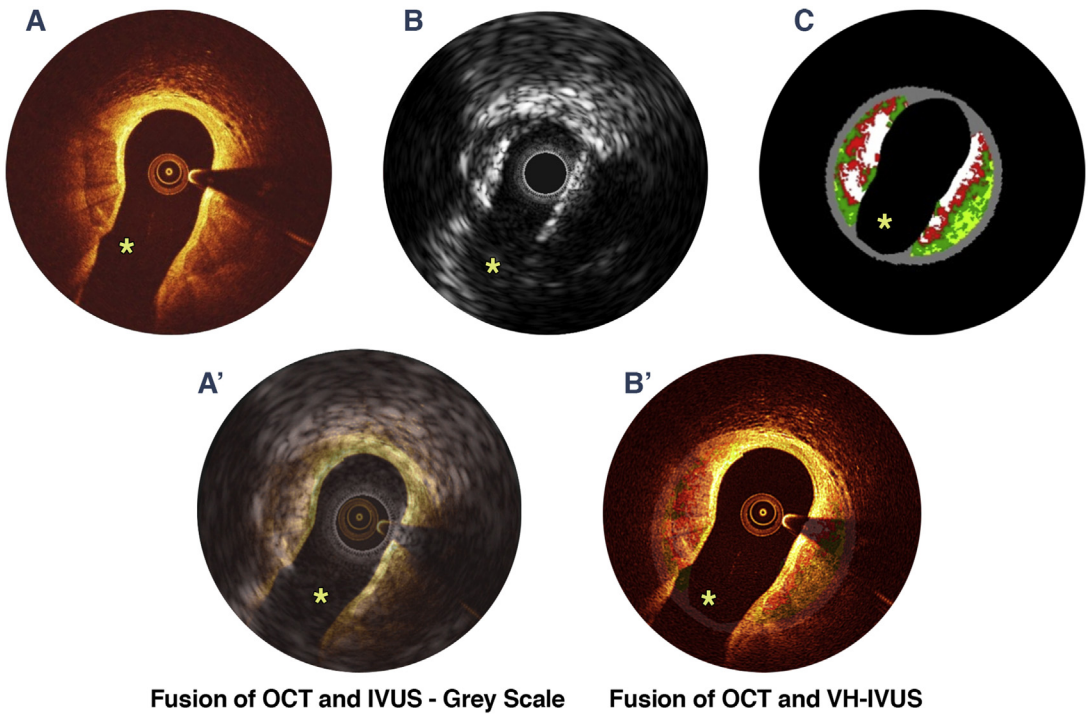

The **yellow asterisk** indicates the side branch. Two calcifications are shown at the ostium of the side branch. Images **A to C** show the matched optical coherence tomography (OCT), grayscale (GS) intravascular ultrasound (IVUS), and IVUS-virtual histology (VH) images using the side branches and 2 calcifications as anatomic landmarks. The **green color** (fibrofatty) in **C** is an artifact of the VH measurement: the ultrasound waves are completely reflected by the calcium, and there is basically no backscattering signal stemming from the shadow area located behind the main ultrasound reflection. Images **A′ and B′** show the fusion images of OCT and GS-IVUS and of OCT and IVUS-VH, respectively.

follow-up was defined as the tissue component constituting approximately 50% in topographically matched calcified area.

MATCHING CROSS SECTION AND ROI DEFINITION. The matching of multimodalities at 1 time point and at follow-up is performed according to the following criteria: the presence of platinum marker (BVS) and common anatomic landmarks such as side branch, vein, pericardium, position and configuration of calcified plaque, characteristic lumen shape and circumferential profile of plaque thickness, and/or positional or directional relationship among all these landmarks (**Figure 1**). The following cross section is not included in the analysis (Online Appendix). The ROI was defined as the scaffold segment and 5 mm proximal and distal.

FUSION CROSS SECTION OF IVUS AND OCT. The principles of fusion imaging have been previously described (8). In summary, the matched GS-IVUS, IVUS-VH, and OCT images were adjusted and fused in Adobe Photoshop Elements 12 (Adobe Systems, San Jose, California) (**Figure 1**). Detailed processes were as follows.

First, the sizes of OCT and IVUS images were adjusted by matching the 1-mm calibration line. The original square shape of both IVUS and OCT images was well defined, so that matching of the 1-mm calibration line between OCT and IVUS images was maintained, thus allowing matching of square image areas.

Second, the 2-dimensional cross-sectional images were rotated using cross-sectional landmarks according to the following hierarchy: 1) side branch; 2) calcification; 3) lumen shape; and 4) circumferential plaques.

Third, to optimize the overlay of IVUS on top of OCT images, the transparency function of Photoshop Elements was used to allow simultaneous visibility of the structures in the underlying OCT images. As a suitable default setting for overlaying IVUS on top of OCT images, transparency of 60% to 70% for the

FIGURE 2 Assessment of Calcification: Calcium Area Was Characterized by the Appearance of Signal-Poor Heterogeneous Images With Sharp Borders

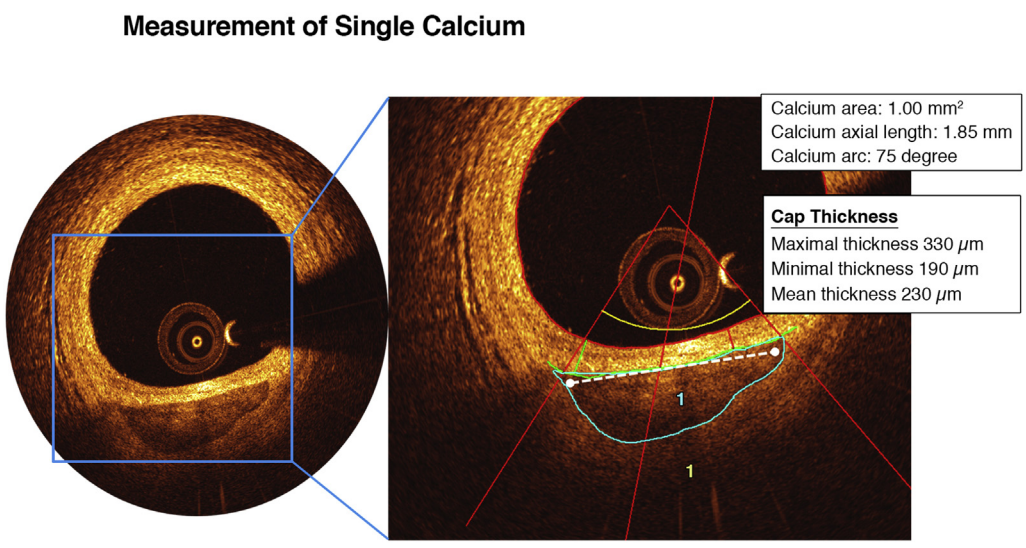

Calcium arc **(yellow)** was measured from the gravitational center of the lumen to the 2 lateral extremities of the calcium. Calcium axial length **(white dashed line)** in each cross section was measured as the maximal geometric length. The maximal **(green)**, minimal **(red)**, and mean cap thickness overlying calcification were measured.

grayscale IVUS images and 70% to 80% for IVUS-VH images was applied.

CALCIUM ASSESSMENT BY FUSION IVUS AND OCT. To assess the diagnostic accuracy of calcium detection of each individual modality compared with the fusion images, the cross sections of each modality were evaluated by 3 teams of 2 cardiologists who were blind to the images of the other modalities at baseline and 5 years using the criteria described earlier.

After having assessed individually the presence or absence of calcification in each imaging modality, a group of 5 cardiologists assessed by consensus the diagnosis of calcification in the matched cross section. Calcification was diagnosed by fusion when qualitative and quantitative criteria were met by at least 2 imaging modalities. Sensitivity and specificity of each modality were determined using the fusion image as comparator.

OCT AND IVUS CALCIFICATION MEASUREMENTS. The following OCT parameters were assessed (Figure 2): calcium area, volume, arc, axial and longitudinal length, and intima thickness overlying calcifications (12); calcium volume was calculated on the basis of the disk summation method (Online Appendix).

AUTOMATIC QUANTITATIVE ECHOGENICITY ANALYSIS. Echogenicity classifies plaque components into 5 categories on the basis of their gray-level intensity on IVUS: calcified, upper-echogenic, hyperechogenic, hypoechogenic, and unknown (13).

STATISTICAL ANALYSIS. Continuous variables are presented as mean ± SD or as median and interquartile range (IQR) as appropriate and were compared using the paired Student *t* test or Wilcoxon signed rank test for baseline versus follow-up comparisons and the independent Student *t* test and Mann-Whitney *U* test for in- versus out-scaffold. Binary variables are summarized as counts and percentages and were compared using the chi-square or Fisher exact test. For each imaging modality alone, sensitivity and specificity for calcium detection were determined using the fusion method as the comparator. Agreement for calcium detection between each modality and the fusion method was assessed using the Cohen κ statistic. Because the data in the study had multilevel structure, a mixed-effects model was used. Patients were implemented as the random effect, and in- or out-scaffold segment was input as the fixed effect. A 2-sided p value <0.05 indicated statistical significance. All analyses were performed using SPSS version 22 (IBM, Armonk, New York).

RESULTS

STUDY POPULATION AND CASE SELECTION. Among 28 patients with complete 5-year follow-up in the

ABSORB Cohort B trial, 15 (16 lesions) with all 3 imaging modalities (GS-IVUS, IVUS-VH, and OCT) available were included in the present analysis. Baseline clinical characteristics of the study population are summarized in Table 1, and IVUS measurements at baseline and 5 years are shown in Table 2. Patients imaged with time-domain OCT were excluded from the analysis (Online Figure 1).

In the 16 coronary lesions, at baseline, 72 cross sections (4.6 ± 1.4 cross sections per lesion) of each of the 3 imaging modalities (IVUS, IVUS-VH, and OCT) were matched and fused using the criteria stated earlier. These fused cross sections were further matched with the corresponding 72 fused cross sections from the 5-year follow-up assessment. These constituted the study database of 72 pairs of matched, fused (GS-IVUS, IVUS-VH, and OCT) cross sections.

No calcification was observed in 33 of these 72 pairs of cross sections (41.8%) (i.e., at neither time point). In the other 39 pairs of fused cross sections (58.2%), 46 calcified area pools were detected at 5-year follow-up. These 46 calcified area pools represented either calcium progression from baseline (n = 24) or de novo calcification (n = 22) (Figure 3).

Of note, calcium was detected by VH only at baseline in 22 cross sections. To definitively determine the true significance of this isolated VH signal, follow-up fusion images were assessed, and calcification was confirmed in 13 of 22 cross sections. In the remaining 9 cross sections, the VH signal of calcification either disappeared or persisted only as an isolated VH signal not confirmed by the fusion method.

DIAGNOSTIC ACCURACY OF CALCIFICATION WITH FUSION AND INDIVIDUAL MODALITIES. Table 3 shows the sensitivity and specificity of each modality in detecting calcium at 2 time points, using the fusion modality as the comparator.

ANALYSIS OF TISSUE PRECURSOR OF CALCIFICATION ON OCT AND IVUS-VH. On IVUS-VH, the tissue precursors of DC at baseline were NC (n = 34 [73.9%]) and fibrous or fibrofatty plaque (n = 5 [10.9%]). In the remaining 7 calcifications (15.2%), calcium was already present at baseline. On OCT, precursors were lipid pool (n = 33 [71.2%]), fibrous plaque (n = 2 [4.3%]), and fibrocalcific tissue (n = 11 [23.9%]).

OCT CALCIUM MEASUREMENTS. An overall increase in calcium area was observed both in-scaffold (Δ = 0.37 mm^2; IQR: 0.25 to 0.74 mm^2) and out-scaffold (Δ = 0.39 mm^2; IQR: 0.21 to 1.2 mm^2) (p = 0.098, in- vs. out-scaffold). The mixed-effects model showed a similar trend (p = 0.117).

Serial changes in intima thickness overlying the calcified plaque as well as axial calcium length and arc were analyzable in 14 plaques (9 in- and 5 out-scaffold) at both time points. Minimal intima thickness overlying calcium increased significantly more for in-scaffold (Δ = 180 ± 152 μm) than out-scaffold (Δ = 16 ± 116 μm) segments (p = 0.034, in- vs. out-scaffold), although it was statistically nonsignificant (p = 0.079) after mixed-effects analysis. Overall, the mean intima thickness, maximal intima thickness, axial calcium length, and arc significantly increased at follow-up, with no differences between in- and out-scaffold segments before and after using the mixed-effects model (Table 4).

Longitudinal calcium length (1.8 ± 0.71 mm at baseline vs. 3.6 ± 2.0 mm at 5 years; p = 0.003) and volume (0.83 ± 0.64 mm^3 at baseline vs. 3.1 ± 2.5 mm^3 at 5 years; p = 0.001) significantly increased at follow-up.

IVUS CALCIFICATION ARC MEASUREMENTS. GS-IVUS detected calcium at both time points in 21 plaques. An

TABLE 1 Baseline Patient Characteristics (15 Patients, 16 Lesions)

Age, yrs	59.14 ± 7.16
Male	9 (60.0)
Hypertension requiring medication	8 (53.3)
Hypercholesterolemia requiring medication	9 (60.0)
Diabetes mellitus requiring medication	0 (0.0)
Myocardial infarction history	4 (26.7)
Cardiac intervention history	2 (13.3)
Current smokers	4 (26.7)
Family history of CHD	10 (66.7)
Clinic presentation	
Stable	12 (80.0)
Non-ST-segment elevation ACS	1 (6.7)
Silent ischemia	0 (0.0)
Target vessel	
Left anterior descending coronary artery	9 (56.2)
Left circumflex coronary artery	3 (18.8)
Right coronary artery	4 (25.0)
AHA/ACC lesion classification	
Type A	0 (0.0)
Type B1	11 (68.8)
Type B2/C	5 (31.3)
Statin use at 5 yrs	14 (93.3)
Rosuvastatin	3 (21.4)
Atorvastatin	7 (50.0)
Simvastatin	5 (35.7)
Lipid profile at 5 yrs (mmol/l)	
Total cholesterol	3.7 ± 0.7
LDL	1.6 ± 0.5
HDL	1.0 ± 0.3
Triglyceride	2.3 ± 0.4

Values are mean ± SD or n (%).

ACC = American College of Cardiology; ACS = acute coronary syndrome; AHA = American Heart Association; CHD = coronary heart disease; HDL = high-density lipoprotein; LDL = low-density lipoprotein.

TABLE 2 Intravascular Ultrasound Measurements at Baseline and 5-Year Follow-Up

	Baseline	5-Year Follow-Up	Difference	p Value
Scaffold segment (16 paired measurements)				
Vessel area, mm^2	14.4 (13.0 to 16.8)	14.2 (11.5 to 15.5)	−0.6 (−1.3 to 0.36)	0.121
Luminal area, mm^2	6.4 (5.8 to 7)	6.3 (5.9 to 7.2)	0.15 (−0.24 to 0.88)	0.352
Plaque area, mm^2	8.4 (6.6 to 10.0)	7.4 (6.2 to 8.5)	−0.82 (−1.5 to −0.24)	0.044
Plaque burden, %	55.8 ± 5.8	52.8 ± 6.1	−3.0 ± 6.7	0.094
Proximal edge (7 paired measurements)				
Vessel area, mm^2	13.5 (12.4 to 14.9)	13.1 (12.1 to 14.8)	−0.28 (−1.0 to 0.06)	0.128
Luminal area, mm^2	8.4 (6.2 to 8.8)	6.2 (5.8 to 8.0)	−0.76 (−1.1 to 0.0)	0.091
Plaque area, mm^2	6.1 (5.8 to 6.2)	6.8 (6.3 to 7.7)	0.54 (0.05 to 0.74)	0.176
Plaque burden, %	43.7 ± 10.3	51.4 ± 6.0	7.8 ± 14.9	0.219
Distal edge (9 paired measurements)				
Vessel area, mm^2	11.1 (9.2 to 15.9)	11.4 (9.9 to 15.0)	−0.31 (−0.68 to 0.64)	0.767
Luminal area, mm^2	6.3 (5.1 to 7.1)	5.7 (5.0 to 6.8)	−0.07 (−1.1 to 0.43)	0.515
Plaque area, mm^2	5.1 (4.2 to 8.4)	5.2 (4.8 to 7.8)	−0.01 (−1.2 to 1.6)	0.953
Plaque burden, %	46.5 ± 14.9	51.2 ± 4.8	4.6 ± 13.5	0.334

Values are median (interquartile range) or mean ± SD.

overall increase in calcium arc was observed, with no difference between in-scaffold ($\Delta = 16 \pm 13°$) and out-scaffold ($\Delta = 35 \pm 28°$) segments ($p = 0.134$, in- vs. out-scaffold), and a similar trend was observed after mixed-effects analysis ($p = 0.075$) (Table 4).

CALCIUM ASSESSMENT WITH IVUS ECHOGENICITY. IVUS echogenicity was evaluated in 39 cross sections containing 46 calcified area pools. An increase in calcium area was observed, with no difference between in-scaffold ($\Delta = 0.21$ mm^2; IQR: 0.1 to 0.28 mm^2) and out-scaffold ($\Delta = 0.22$ mm^2; IQR: 0.03 0.37 mm^2) segments ($p = 0.881$, in- vs. out-scaffold); after applying the mixed-effects model, $p = 0.887$ (Online Table 1).

DISCUSSION

The findings of the present study can be summarized as follows: 1) fusion OCT and IVUS images provide a comprehensive assessment of coronary artery calcification; 2) calcification progresses to a similar extent in in-scaffold and out-scaffold segments, suggesting that calcification is a global phenomenon not influenced by the presence of the scaffold; 3) the intima thickness overlying calcium in-scaffold is thicker than out-scaffold segments and may constitute a new endoluminal lining isolating the calcified plaque from the lumen; 4) IVUS-VH has high sensitivity for the detection of calcification; and 5) lipid pool and NC are the most frequent precursors of calcifications at follow-up.

FIGURE 3 Flowchart for Cross Section Selection

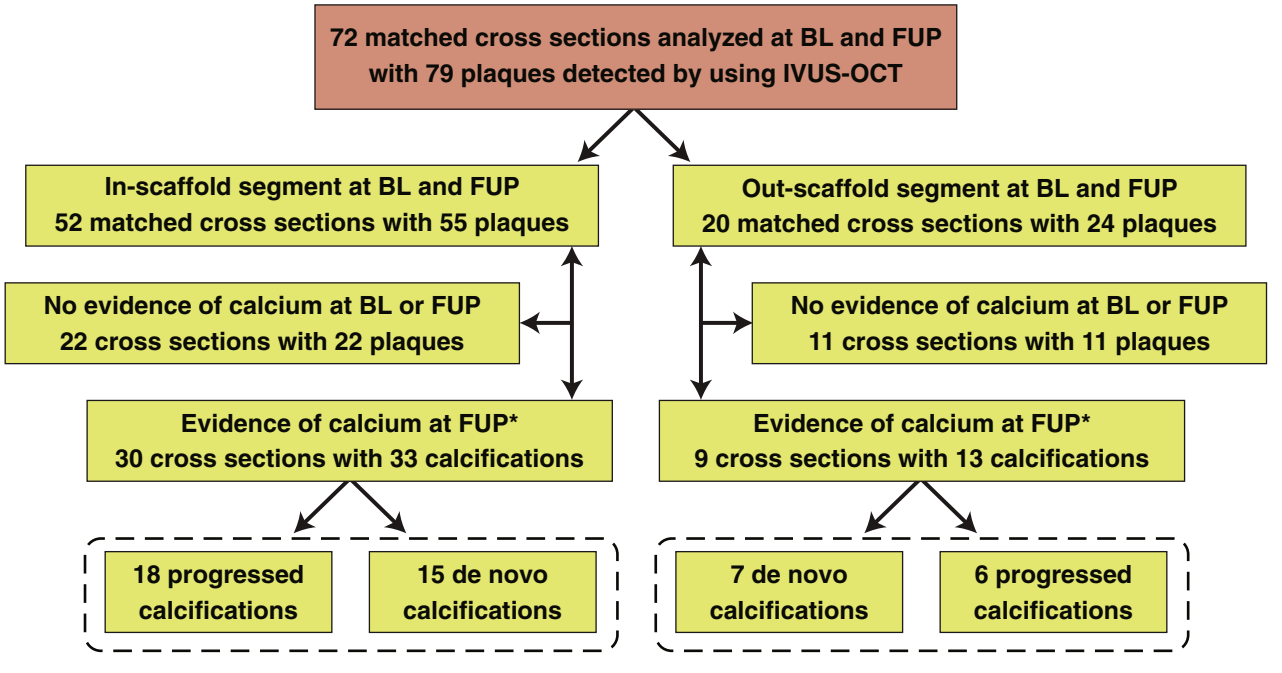

Seventy-two cross section (79 pools) matched for grayscale intravascular ultrasound (IVUS), IVUS-virtual histology, and optical coherence tomography (OCT) images at baseline and follow-up were analyzed. *No calcification was observed at baseline (BL) that was present at follow-up (FUP).

CALCIFICATION DETECTION WITH FUSION OF OCT AND IVUS. Coronary artery calcium affects the pathophysiologic development of atherosclerosis and triggers cardiac events. In addition, its severity and endoluminal topography affect interventional strategy and clinical events (14). In the present study, calcification was evaluated by fusion of OCT, GS-IVUS, and IVUS-VH, which improved the diagnostic accuracy of calcification by combining the individual strengths of each modality. As for the diagnostic accuracy of individual modalities in detecting calcification, GS-IVUS at baseline showed lower sensitivity than IVUS-VH, which could be explained by the fact that the complex classification tree and algorithm for tissue analysis on IVUS-VH relies on backscattering of the radiofrequency signal, whereas GS-IVUS detects only the envelope of the ultrasonic signal.

In this analysis, the specificity of OCT was high, but the sensitivity was limited. Among possible reasons for the low sensitivity are the limited penetration of OCT, which precludes the detection of deep calcium deposits, guidewire artifacts, and tangential signal dropout.

IVUS-VH, however, showed 100% sensitivity and low specificity for calcium detection. Some isolated, localized IVUS-VH DC signals at baseline were considered artifacts when not confirmed by grayscale and/or OCT calcium detection. Interestingly, some of these isolated VH signals (13 of 22) became fully calcified plaques at follow-up in the same topographic area detected using the fusion method (**Figure 4**). This unexpected finding might reopen the debate on the diagnostic value of IVUS-VH for the detection of calcium (15,16). The validation study with IVUS-VH obtained from 45-MHz rotation IVUS has demonstrated the capacity of the VH algorithm to detect microcalcification in ROIs as small as 0.25 × 0.25 mm (3).

CALCIFIED PLAQUE DEVELOPMENT AND PRECURSORS. In the present study, calcifications (calcium area, arc, axial length, calcified echogenicity) were shown to increase to a similar extent in both in- and out-scaffold segments. This implies a global calcification phenomenon unrelated to the implantation of the scaffold. Calcium progression has been shown in patients on secondary prevention and statin treatment (17). This natural history is thought to reflect a plaque-stabilizing phenomenon associated with lipid-lowering therapy (18).

Previous data have shown indirectly that at follow-up, atherosclerosis regresses by decreasing its NC content and increasing its DC content on average (17–19). Our study is the first to date to clearly and directly demonstrate that phenomenon at the plaque and cross section level. Only by this meticulous paired, matched analysis of in vivo data with long-term follow-up were we able to demonstrate the transformation of NC into calcium, as the vast majority of tissue precursors were NC or lipid pool. The molecular mechanisms for this transformation remain largely unclear, but "mineral deposit," "osteoprotegerin," and efferocytosis of macrophage are the possible mechanisms (20,21). Coregistration of multislice computed tomography and fluoride-18 positron emission tomography has clearly demonstrated dynamic and inflammatory changes in calcified lesions. Fluoride is taken up by macrophages, liposomes, and microcalcification. In addition, NC on IVUS-VH has been colocalized with calcification visualized by multislice computed tomography and fluoride-18 positron emission tomography (22).

TABLE 3 Diagnostic Accuracy of Individual Optical Coherence Tomography, Grayscale Intravascular Ultrasound, and Intravascular Ultrasound-Virtual Histology for the Calcification Detection of Coronary Atherosclerotic Plaque at Baseline and 5-Year Follow-Up: Comparison With Fusion Method

			Sensitivity, %	Specificity, %	κ	p Value
Pooled baseline and 5-yr						
OCT	OCT(−)	OCT(+)				
Fusion(−)	88	0	70.0	100.0	0.722	<0.001
Fusion(+)	21	49				
GS-IVUS	GS-IVUS(−)	GS-IVUS(+)				
Fusion(−)	88	0	95.7	100.0	0.961	<0.001
Fusion(+)	3	67				
IVUS-VH	IVUS-VH(−)	IVUS-VH(+)				
Fusion(−)	62	26	100.0	70.5	0.679	<0.001
Fusion(+)	0	70				
Baseline						
OCT	OCT(−)	OCT(+)				
Fusion(−)	55	0	58.3	100.0	0.661	<0.001
Fusion(+)	10	14				
GS-IVUS	GS-IVUS(−)	GS- IVUS(+)				
Fusion(−)	55	0	87.5	100.0	0.907	<0.001
Fusion(+)	3	21				
IVUS	IVUS-VH(−)	IVUS-VH(+)				
Fusion(−)	33	22	100.0	60.0	0.477	<0.001
Fusion(+)	0	24				
5-yr						
OCT	OCT(−)	OCT(+)				
Fusion(−)	33	0	76.1	100.0	0.727	<0.001
Fusion(+)	11	35				
GS-IVUS	GS-IVUS(−)	GS-IVUS(+)				
Fusion(−)	33	0	100.0	100.0	1.00	<0.001
Fusion(+)	0	46				
IVUS-VH	IVUS-VH(−)	IVUS-VH(+)				
Fusion(−)	29	4	100.0	87.9	0.894	<0.001
Fusion(+)	0	46				

Values are n (%).
GS = grayscale; IVUS = intravascular ultrasound; OCT = optical coherence tomography; VH = virtual histology.

TABLE 4 Evolution From Baseline to 5-Year Follow-Up of 46 Calcifications Detected by Fusion at Follow-Up in 39 Cross Sections

	Baseline	5-Year	Difference	p Value
Calcium area (n = 46) measured on OCT in de novo or progressed calcifications				
Calcium area, mm^2				
In-scaffold (n = 33)	0.22 ± 0.32	0.70 ± 0.41	0.48 ± 0.32	<0.001
Out-scaffold (n = 13)	0.19 ± 0.30	1.04 ± 1.14	0.85 ± 1.0	0.003
p value, in- vs. out-scaffold	0.774	0.199	0.098	
n = 14 progressed calcifications detectable on OCT				
Minimal intima thickness overlying calcium, μm				
In-scaffold (n = 9)	92 ± 53	272 ± 149	180 ± 152	0.002
Out-scaffold (n = 5)	223 ± 156	239 ± 119	16 ± 116	0.345
p value, in- vs. out-scaffold	0.031	0.629	0.034	
Maximal intima thickness overlying calcium, μm				
In-scaffold (n = 9)	303 (181–480)	355 (254–519)	95 (40–283)	0.209
Out-scaffold (n = 5)	248 (141–333)	278 (204–447)	55 (24–87)	0.345
p value, in- vs. out-scaffold	0.482	0.274	0.16	
Mean intima thickness overlying calcium, μm				
In-scaffold (n = 9)	217 ± 117	361 ± 183	144 ± 141	0.005
Out-scaffold (n = 5)	238 ± 111	265 ± 109	27 ± 38	0.147
p value, in- vs. out-scaffold	0.721	0.310	0.066	
Arc on OCT, °				
In-scaffold (n = 9)	30 ± 13	46 ± 17	16 ± 14	0.003
Out-scaffold (n = 5)	34 ± 24	70 ± 19	36 ± 30	0.03
p value, in- vs. out-scaffold	0.694	0.139	0.057	
Axial length, mm				
In-scaffold (n = 9)	0.89 (0.51–1.08)	1.1 (0.64–1.4)	0.42 (0.17–0.77)	0.002
Out-scaffold (n = 5)	0.53 (0.38–0.79)	0.95 (0.70–1.2)	0.45 (0.1–1.2)	0.028
p value, in- vs. out-scaffold	0.261	0.936	0.851	
Calcium volume and longitudinal length assessed in 13 progressed calcifications detectable on OCT*				
Longitudinal length, mm (n = 13)	1.8 ± 0.71	3.6 ± 2.0	1.7 ± 2.0	0.003
Volume, mm^3 (n = 13)	0.83 ± 0.64	3.1 ± 2.5	2.3 ± 2.4	0.001
n = 21 progressed calcifications detectable on IVUS				
Arc on IVUS, deg				
In-scaffold (n = 16)	43 ± 21	59 ± 23	16 ± 13	0.002
Out-scaffold (n = 5)	34 ± 24	69 ± 31	35 ± 28	0.018
p value, in- vs. out-scaffold	0.350	0.442	0.134	

Fourteen progressed calcifications detectable on OCT and 21 detectable on grayscale IVUS at both time points. Values are mean ± SD or median (interquartile range).
*Thirteen separate calcified volumes were quantified by OCT; 2 continuous calcified cross sections belong to one continuous calcified volume.
IVUS = intravascular ultrasound; OCT = optical coherence tomography.

Regulatory bodies in Europe and the United States have raised concerns over bioresorption of fully bioresorbable scaffold in polylactide: local acidification and transient detection (Von Kossa staining) of calcification around the degraded scaffold strut have been reported in preclinical models as early as 28 days but had disappeared at long-term follow-up (23). Despite these reassuring preclinical data, clinicians remain concerned by the long-term outcomes of polylactide bioresorbable scaffolds. For instance, in preclinical studies, it has been demonstrated that metallic bioresorbable scaffolds in magnesium evolve into soft amorphous hydroxyapatite of calcium (24).

The progression and development of new calcified plaque should not be confused with neoatherosclerosis, whose OCT features are very specific (25). It must be emphasized that the luminal area in the present series was 6.4 mm^2 at baseline and 6.3 mm^2 at 5 years, with no sign of restenosis or luminal encroachment (Table 2).

RE-CAPPING OF THE CALCIFIED PLAQUE. Despite the appearance and progression of calcifications, the new lesions could be considered stable for the following reasons: at 5-year follow-up, a moderately thick layer of neointima (272 ± 149 μm) is located on top of each calcified plaque in-scaffold segment (Figures 4D and 4F′). The minimal intima thickness overlying the calcification increased significantly more in in-scaffold segments at 5-year follow-up compared with out-scaffold segments. The term

FIGURE 4 **Serial Analyses of a Calcification by Fusion of Optical Coherence Tomography and Intravascular Ultrasound Images at Baseline and Follow-Up**

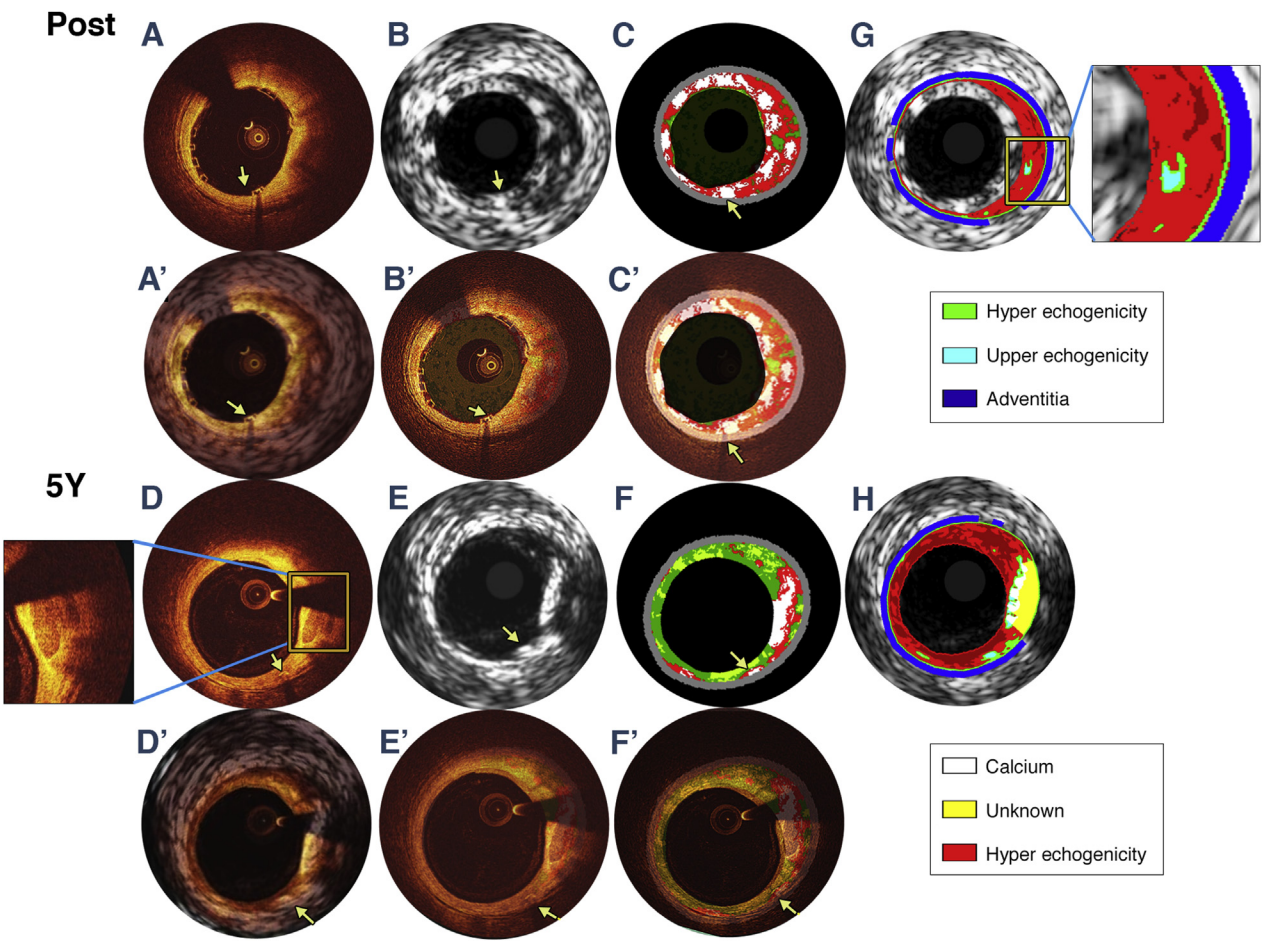

The **yellow arrow** indicates the platinum marker at 6 o'clock. Images **A to C** show the matched cross section of optical coherence tomography (OCT), grayscale (GS) intravascular ultrasound (IVUS), and IVUS-virtual histology (VH) at baseline, whereas images **D to F** show matched cross sections at follow-up. Image **A**, at 1 to 5 o'clock, shows a lipid-pool plaque with low light intensity, high light attenuation, and an unclear border. Image **(C)** shows mixed plaque composition of necrotic core, fibrous tissue, and dense calcium; struts on IVUS-VH are identified as pseudo dense calcium. Images **(A′)** and **(B′)** show the fusion of OCT and GS-IVUS and of OCT and IVUS-VH, respectively. Image **C′** emphasizes the VH information of image **B′** by selecting a lower threshold of transparency. The calcium spot with sharp borders **(D)** corresponds to the lipid-rich plaque on image **A**. Images **D′ and E′** show the fusion of OCT and GS-IVUS and of OCT and IVUS-VH, respectively. Image **F′** emphasizes the VH information of image **E′** by selecting a lower threshold of transparency. Image **G** shows the echogenicity analysis behind the strut at baseline, upper-echogenicity with **light blue color** progressed to calcium at follow-up **(H; white)**. The color legend for each echogenicity classification is provided.

"re-capping of the plaque" has been coined to describe this phenomenon (12).

This "cap" overlying the calcification is likely due to the integration of the polymeric struts into the vessel wall, which isolates the lumen from the underlying calcium and the surrounding lipid and NC. The "cap" may transform the unstable phenotype of plaque to a stable one by covering the calcific spots and thin-cap fibroatheroma with neointima (12); furthermore, calcium with a homogenous thick cap will have less effect on the shear stress than spotty superficial calcium (26).

STUDY LIMITATIONS. This study represents the longest natural history of evolution of plaques analyzed serially by fusion IVUS and OCT. There were nevertheless some methodological limitations. First, precise and careful matching of images acquired with a sampling rate as different as 1 frame/s from VH to 100 or 180 frames/s for OCT considerably reduces the number of analyzable cross sections per lesion. The goal of the study was not to unravel clinical implications but to generate hypotheses. Therefore caution should be exercised when extrapolating the study results given the limited number of cross sections.

Second, the lack of intracoronary images pre-procedure renders the analysis of true tissue composition more complex, because strut artifacts are detected as "pseudo" DC and NC on IVUS-VH images. To account for that, we excluded struts from the IVUS images according to a previously validated method (10).

Third, we did not use any automated imaging software specifically validated to create fused images. Therefore, the display of the presented images is purely exploratory but may serve as a preamble for further development of dedicated software application on imaging on the basis of photoacoustic systems (27), as well as hybrid technique (28).

Fourth, the data on lipid profiles and medications in this study were collected as general clinical information. It was clearly stipulated in the protocol that the investigators had to follow the guidelines of the European Society of Cardiology (at the time of the trial design, target low-density lipoprotein <2 mmol/l). In the present study at 5 years, 14 of 15 patients were treated with hydroxymethylglutaryl coenzyme-A reductase inhibitors (3 with rosuvastatin, 7 with atorvastatin, and 5 with simvastatin). Low-density lipoprotein was well controlled and decreased from baseline (2.6 ± 0.5 mmol/l) to 5 years (1.6 ± 0.5 mmol/l). All 15 patients presented with at least 1 calcification in the selected 72 fused cross sections. The limited number of observations does not allow any physiopathological or pharmacological interpretation.

Fifth, our findings are limited to segments treated with BVS and cannot be extrapolated to segments treated with metallic stents or untreated ones. Of note, because the struts get resorbed at about 2 years of follow-up, we can speculate that at 5 years, the behavior of the vascular wall should be close to that of an untreated segment.

Finally, because no validation against histologic findings was performed, our results should be cautiously interpreted as hypothesis generating regarding the potential benefits of hybrid imaging techniques.

CONCLUSIONS

With the use of OCT and IVUS fusion imaging, we demonstrate in vivo similar calcium growth in in-scaffold and out-scaffold segments in patients treated with BVS. NC is the most frequent precursor of calcification. The scaffold resorption process creates a tissue layer that re-caps calcified plaques.

ACKNOWLEDGMENT The authors thank H.M. Garcia-Garcia for his work in the core laboratory for many years, including the analysis used in the present work.

ADDRESS FOR CORRESPONDENCE: Prof. Dr. Patrick W. Serruys, Westblaak 98, 3012KM, Rotterdam, the Netherlands. E-mail: patrick.w.j.c.serruys@gmail.com.

PERSPECTIVES

COMPETENCY IN MEDICAL KNOWLEDGE: Both OCT and IVUS alone have limitations in evaluating calcification. In this study, by fusing OCT and IVUS, we have shown that similar calcium growth in in-scaffold and out-scaffold segments in patients treated with BVS. NC is the most frequent precursor of calcification.

TRANSLATIONAL OUTLOOK: In the future, coregistration of OCT and IVUS techniques (e.g., acquisition with hybrid catheters) will likely be in clinical practice. Future research is needed to define whether calcification is a sign of plaque progression or stabilization of coronary atherosclerosis. Remaining questions include ascertaining the molecular mechanism and determining how to use pharmacological intervention targeting calcification to stabilize the plaque.

REFERENCES

1. Shan P, Mintz GS, McPherson JA, et al. Usefulness of coronary atheroma burden to predict cardiovascular events in patients presenting with acute coronary syndromes (from the PROSPECT Study). Am J Cardiol 2015;116:1672–7.

2. Mintz GS, Nissen SE, Anderson WD, et al. American College of Cardiology clinical expert consensus document on standards for acquisition, measurement and reporting of intravascular ultrasound studies (IVUS). A report of the American College of Cardiology Task Force on Clinical Expert Consensus Documents. J Am Coll Cardiol 2001;37:1478–92.

3. Campos CM, Fedewa RJ, Garcia-Garcia HM, et al. Ex vivo validation of 45 MHz intravascular ultrasound backscatter tissue characterization. Eur Heart J Cardiovasc Imaging 2015;16:1112–9.

4. Tolle M, Reshetnik A, Schuchardt M, Hohne M, van der Giet M. Arteriosclerosis and vascular calcification: causes, clinical assessment and therapy. Eur J Clin Invest 2015;45:976–85.

5. Kume T, Okura H, Kawamoto T, et al. Assessment of the coronary calcification by optical coherence tomography. Eurointervention 2011;6:768–72.

6. Kubo T, Imanishi T, Takarada S, et al. Assessment of culprit lesion morphology in acute myocardial infarction: ability of optical coherence tomography compared with intravascular ultrasound and coronary angioscopy. J Am Coll Cardiol 2007;50:933–9.

7. Gonzalo N, Garcia-Garcia HM, Regar E, et al. In vivo assessment of high-risk coronary plaques at bifurcations with combined intravascular ultrasound and optical coherence tomography. J Am Coll Cardiol Img 2009;2:473–82.

8. Raber L, Heo JH, Radu MD, et al. Offline fusion of co-registered intravascular ultrasound and frequency domain optical coherence tomography images for the analysis of human atherosclerotic plaques. Eurointervention 2012;8:98–108.

9. Serruys PW, Ormiston J, van Geuns RJ, et al. A polylactide bioresorbable scaffold eluting everolimus for treatment of coronary stenosis: 5-year follow-up. J Am Coll Cardiol 2016;67:766–76.

10. Brugaletta S, Garcia-Garcia HM, Garg S, et al. Temporal changes of coronary artery plaque located behind the struts of the everolimus eluting bioresorbable vascular scaffold. Int J Cardiovasc Imaging 2011;27:859–66.

11. Tearney GJ, Regar E, Akasaka T, et al. Consensus standards for acquisition, measurement, and reporting of intravascular optical coherence tomography studies: a report from the International Working Group for Intravascular Optical Coherence Tomography Standardization and Validation. J Am Coll Cardiol 2012;59:1058–72.

12. Bourantas CV, Serruys PW, Nakatani S, et al. Bioresorbable vascular scaffold treatment induces the formation of neointimal cap that seals the underlying plaque without compromising the luminal dimensions: a concept based on serial optical coherence tomography data. Eurointervention 2014;11:746–56.

13. Campos CM, Ishibashi Y, Eggermont J, et al. Echogenicity as a surrogate for bioresorbable everolimus-eluting scaffold degradation: analysis at 1-, 3-, 6-, 12-18, 24-, 30-, 36- and 42-month follow-up in a porcine model. Int J Cardiovasc Imaging 2015;31:471–82.

14. Mintz GS. Intravascular imaging of coronary calcification and its clinical implications. J Am Coll Cardiol Img 2015;8:461–71.

15. Stone GW, Mintz GS. Letter by Stone and Mintz regarding article, "Unreliable assessment of necrotic core by virtual histology intravascular ultrasound in porcine coronary artery disease." Circ Cardiovasc Imaging 2010;3:e4.

16. Thim T, Hagensen MK, Wallace-Bradley D, et al. Unreliable assessment of necrotic core by virtual histology intravascular ultrasound in porcine coronary artery disease. Circ Cardiovasc Imaging 2010;3:384–91.

17. Nasu K, Tsuchikane E, Katoh O, et al. Effect of fluvastatin on progression of coronary atherosclerotic plaque evaluated by virtual histology intravascular ultrasound. J Am Coll Cardiol Intv 2009;2:689–96.

18. Raber L, Taniwaki M, Zaugg S, et al. Effect of high-intensity statin therapy on atherosclerosis in non-infarct-related coronary arteries (IBIS-4): a serial intravascular ultrasonography study. Eur Heart J 2015;36:490–500.

19. Banach M, Serban C, Sahebkar A, et al. Impact of statin therapy on coronary plaque composition: a systematic review and meta-analysis of virtual histology intravascular ultrasound studies. BMC Med 2015;13:229.

20. Otsuka F, Sakakura K, Yahagi K, Joner M, Virmani R. Has our understanding of calcification in human coronary atherosclerosis progressed? Arterioscler Thromb Vasc Biol 2014;34:724–36.

21. Van Campenhout A, Golledge J. Osteoprotegerin, vascular calcification and atherosclerosis. Atherosclerosis 2009;204:321–9.

22. Doris MK, Newby DE. Identification of early vascular calcification with F-sodium fluoride: potential clinical application. Expert Rev Cardiovasc Ther 2016;(6):1–11.

23. Onuma Y, Serruys PW, Perkins LE, et al. Intracoronary optical coherence tomography and histology at 1 month and 2, 3, and 4 years after implantation of everolimus-eluting bioresorbable vascular scaffolds in a porcine coronary artery model: an attempt to decipher the human optical coherence tomography images in the ABSORB trial. Circulation 2010;122:2288–300.

24. Campos CM, Muramatsu T, Iqbal J, et al. Bioresorbable drug-eluting magnesium-alloy scaffold for treatment of coronary artery disease. Int J Mol Sci 2013;14:24492–500.

25. Taniwaki M, Windecker S, Zaugg S, et al. The association between in-stent neoatherosclerosis and native coronary artery disease progression: a long-term angiographic and optical coherence tomography cohort study. Eur Heart J 2015;36:2167–76.

26. Vengrenyuk Y, Carlier S, Xanthos S, et al. A hypothesis for vulnerable plaque rupture due to stress-induced debonding around cellular microcalcifications in thin fibrous caps. Proc Natl Acad Sci U S A 2006;103:14678–83.

27. Kim J, Lee D, Jung U, Kim C. Photoacoustic imaging platforms for multimodal imaging. Ultrasonography 2015;34:88–97.

28. Bourantas CV, Jaffer FA, Gijsen FJ, et al. Hybrid intravascular imaging: recent advances, technical considerations, and current applications in the study of plaque pathophysiology. Eur Heart J 2017;38:400–12.

KEY WORDS bioresorbable vascular scaffold, calcification, fusion

APPENDIX For supplemental methods, results, figures, and tables, please see the online version of this article.